40th AIAA/ASME/SAE/ASEE Joint Propulsion Conference and Exhibit
11 - 14 July 2004, Fort Lauderdale, Florida

AIAA 2004-3951

A Comparison of 2-D Hybrid Hall Thruster Model to Experimental Measurements

Michelle K. Allis,[*] Nicolas Gascon,[†] Caroline Vialard-Goudou,[‡] and Mark A. Cappelli[§]
Stanford University, Stanford, CA, 94305

and

Eduardo Fernandez[**]
Eckerd College, St. Petersburg, Florida, 33711

A two-dimensional hybrid particle-in-cell numerical model has been constructed in the radial-axial plane with the intent of examining the physics governing Hall thruster operation. The electrons are treated as a magnetized quasi-one-dimensional fluid and the ions are treated as collisionless, nonmagnetized discrete particles. The anomalously high electron conductivity experimentally observed in Hall thrusters is accounted for using experimental measurements in the Stanford Hall thruster. An evaluation is made of differing treatments of electron mobility, background gas, neutral wall interactions, and charge exchange collisions. The results are compared to experimental measurements of ion and neutral number densities and velocities, electron temperature, and electric potential.

Nomenclature

B	=	magnetic field
e	=	electron charge
E	=	electric field
g	=	relative velocity
I_a	=	discharge current
J	=	current density
k	=	Boltzmann constant
K	=	thermal diffusivity
$n_{e,i}$	=	plasma/ion density
n_n	=	neutral density
S	=	channel cross section
T_e	=	electron temperature
u	=	velocity
ϕ	=	electric potential
ϕ^*	=	thermalized electric potential
φ	=	ion production cost
μ	=	electron cross-field mobility
σ	=	total cross section
τ	=	mean time between collisions
ω_{ce}	=	electron gyrofrequency

[*] Research Assistant, Mechanical Engineering Department, Building 520. Member, AIAA.
[†] Post-Doctoral Research Associate, Mechanical Engineering Department, Building 520. Member, AIAA.
[‡] Research Assistant, Mechanical Engineering Department, Building 520. Member, AIAA.
[§] Associate Professor, Mechanical Engineering Department, Building 520. Member, AIAA.
[**] Assistant Professor, Natural Sciences.

I. Introduction

Closed drift thrusters are an electric propulsion technology receiving considerable attention for their low thrust applications. The Hall thruster is ideally suited for performing low thrust maneuvers such as satellite station keeping and orbit transfer. Thrust is typically produced by accelerating ions through an electric field in an annular plasma. The electric potential is maintained between an external cathode and an anode at the base of the channel. Imposing a radial magnetic field causes a region of high resistance in the electron path due to the Hall current, which creates a zone of high ionization and strong electric field near the exit of the thruster.

There are numerous reasons for developing computer simulations of Hall thrusters. One important motivation for modeling plasma propulsion devices is to quantify the relationship between high velocity ions created by the thruster and spacecraft degradation. Backflow of energetic ions from the plume due to flow divergence and charge exchange collisions may cause sputtering of spacecraft surfaces and deposition of sputtered material onto critical spacecraft components such as solar panels. Another negative consequence of high energy ions is that the creation of these particles inside the thruster can lead to serious erosion of the channel walls. An accurate simulation of Hall thrusters is necessary to predict the effect of these interactions in a space environment.

In addition to understanding spacecraft contamination effects, other motivations for a numerical model include thruster optimization, simulation of space conditions, and development of a tool to aid in the design of future experiments. However, before a Hall thruster simulation can be confidently employed for any of these purposes, the plasma dynamics that form the basis of thruster operation must be well understood.

Currently, there are two primary branches of Hall thruster models: those that deal with the thruster plume and those that simulate the interior channel of the thruster. Frequently, the end result of channel flow model will be used as a boundary condition for a plume model. The present study is of the type concerned with the interior of the Hall thruster and the near-field plume region. A 2-D hybrid particle-fluid simulation in the radial and axial plane has been constructed in order to develop a better understanding of complex physics-related issues in Hall thruster dynamics.

A primary challenge in the modeling of channel flow is the treatment of the poorly understood electron conductivity. Since the mobility of electrons affects both the rate of ionization and the accelerating potential, accurately modeling the transport mechanism is critical to developing a practical simulation. However, the experimentally measured mobility of a Hall thruster substantially exceeds the classical value based on electron-neutral collisions. Two possible mechanisms for this anomalous transport are electron wall interactions and azimuthal fluctuations in electron density. Since the 2-D code can not capture the aziumuthal dynamics, ad-hoc transport models are imposed based on Bohm diffusion, which scales as the inverse of the magnetic field. In the present study, a comparison is made between a constant Bohm transport coefficient and an experimentally-motivated axially dependent coefficient. Additionally, this paper examines the effect of neutral wall interactions, background gas, and charge exchange collisions on numerical results. Comparisons are then made between the simulation and experimental data in order to assess the validity of the model.

II. Numerical Model

A. Assumptions

To aid in the understanding of Hall thruster dynamics, a two dimensional model has been constructed in the radial-axial plane[1] similar to the model described by Fife[2,3]. The hybrid model employs a quasi-one-dimensional fluid treatment of electrons and a particle-in-cell (PIC) treatment of the heavy species, Xe and Xe^+. Since the Debye length of a typical Hall thruster plasma is smaller than the length scales of interest, the two solutions are coupled assuming space charge neutrality.

The computational geometry used in the simulation corresponds to the Stanford Hall Thruster given that extensive experimental data exists for comparison purposes. The annular channel is approximately 8 cm in length and 1.2 cm in width. The insulating channel walls are made of alumina. A mass flow rate of 2 mg/s is implemented in the model to match experimental conditions.

Measurements of the magnetic field along the channel centerline are used to impose a constant external magnetic field as shown in Fig. 1. It is assumed that the discharge does not significantly affect the shape or strength of the field. The radial variation of the magnetic field is obtained by solving Laplace's equation for the magnetic potential after specifying the location of the magnetic poles and assuming infinite permeability of the pole pieces. Due to high electron conductivity parallel to the field lines, the electron temperature is assumed to be uniform along magnetic contours.

In addition to employing experimental magnetic field measurements in the simulation, an experimentally-based effective mobility is used to account for anomalously high cross-field transport due to azimuthal fluctuations and

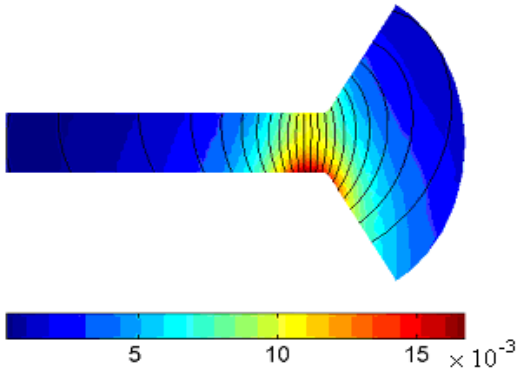

Figure 1. Magnetic field strength [Tesla] and contour lines of Stanford Hall Thruster.

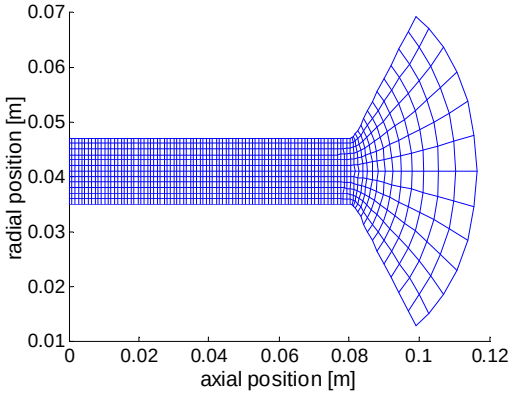

Figure 2. Computational grid of Stanford Hall thruster radial-axial simulation

near-wall conductivity. However, due to limited experimental data, the implemented transport coefficient is currently radially uniform and extrapolated near the anode.

B. Neutrals

Neutral xenon particles are injected from a region near the center of the anode according to a prescribed mass flow rate of 2 mg/s. The introduced particle velocity distribution is assumed to be that of a Maxwellian one-way flux[4] corresponding to the anode temperature of 1000K. Sonic injection does not significantly affect results downstream of the anode. However, diffuse injection is assumed to be more realistic and will therefore be the only injection scheme presented. Azimuthal components of velocity are not included in the 2-D simulation.

Since neutral particles are not affected by electric and magnetic fields, only the particle positions are updated at each time step, while the velocity components remain the same. Particles which exit the computational domain along the channel walls are reflected back into the domain. It is assumed that particles that impact the channel walls thermalize at the wall temperature and are diffusely scattered back into the channel. Similar to anode injection, the velocity distribution is assumed to be half-Maxwellian. Particles which exit the computational domain in the plume region are no longer tracked by the simulation.

C. Ions

Singly-charged xenon ions are generated through electron impact ionization of neutral atoms. The ionization rate is calculated as a function of electron temperature by assuming Maxwellian electrons and using experimental cross section data reported in the Siglo database. In addition to increasing the ion population, the ionization process simultaneously depletes the neutral population at each time step. In the present model, only singly-charged ions are considered.

Due to their large inertia and Larmor radius, ions are not significantly affected by the external magnetic field. Therefore, the equation of motion used to update ion velocities at each time step only includes a force due to the transient, spatially varying electric field. Similar to the neutral treatment, ions leave the simulation after crossing the computational boundaries in the plume. Ions which impact channel walls recombine to form neutrals and are scattered diffusely using a half-Maxwellian velocity distribution.

D. Electrons

As outlined by Fife, the electron fluid is governed by the first three moments of the Boltzmann equation in addition to a current conservation equation, assuming quasineutrality.

Neglecting inertial terms and collisional effects, the momentum equation parallel to the magnetic field describes a balance between electric and pressure forces. Integrating along an isothermal magnetic contour yields an expression for the electric potential, ϕ.

$$\phi = \frac{kT_e}{e}\ln(n_e) + \phi^* \tag{1}$$

where ϕ^* is the thermalized electric potential, k is the Boltzmann constant, e is the charge of an electron, T_e is the electron temperature, and n_e is the plasma density. The electric field, E, is then given everywhere in the domain by:

$$E = -\nabla\phi \tag{2}$$

Perpendicular to the magnetic contours, the electron momentum equation balances electric, pressure, and collisional drag forces. Once again inertial terms are ignored. An **E**×**B** axial force produced by azimuthal electric potential fluctuations interacting with the radial magnetic field is not directly captured in the 2-D simulation. However, this additional contribution to axial force is included through an effective mobility and diffusivity in the generalized Ohm's law:

$$u_{e\hat{n}} = -\mu\left(E_{\hat{n}} + \frac{kT_e}{en_e}\frac{\partial n_e}{\partial\hat{n}} + \frac{k}{e}\frac{\partial T_e}{\partial\hat{n}}\right) \tag{3}$$

where $\hat{n}$ indicates the direction normal to the magnetic field, $u_{e\hat{n}}$ is the electron velocity in the normal direction, and μ is the effective mobility.

A transient, spatially varying electron temperature is determined using the second moment of the Boltzmann equation characterizing energy transport:

$$\frac{\partial}{\partial t}\left(\frac{3}{2}n_e kT_e\right) + \frac{\partial}{\partial\hat{n}}\left(\frac{5}{2}n_e u_{e\hat{n}} kT_e - K\frac{\partial T_e}{\partial\hat{n}}\right) = -\dot{n}_e\varphi(T_e)E_i - \alpha T_e^{3/2} + j_{e\hat{n}}E_{\hat{n}} \tag{4}$$

In the above expression, K is the thermal diffusivity, which incorporates the anomalous electron transport coefficient. The ion production cost, $\varphi(T_e)$, is fit using an exponential expression given by Dugan[5], and is evolved in the original nonlinear form. The terms on the right hand side of Eq. (4) represent the ionization and wall damping sink terms and the joule heating source term. Presently, the wall damping model is based on a constant secondary electron emission coefficient of 0.6 with an ad hoc factor included in the coefficient, α, to lower the damping near the anode for simulation stability.

Assuming space charge neutrality, the electron density, n_e, is everywhere equal to the ion density, n_i. In order to enforce electron continuity, a total discharge current conservation constraint is imposed:

$$I_a = \int_A n_e\left(u_{i\hat{n}} - u_{e\hat{n}}\right)dS \tag{5}$$

where S is the channel cross section.

Substitution of the expression for perpendicular electron velocity given by Eq. (3) into the current conservation equation yields an expression for the thermalized potential, ϕ^*, in terms of electron temperature. Therefore, by obtaining the electron temperature through direct solution of the energy equation, the spatially-varying electric field, electron velocity, and ionization rate can be calculated at each time step.

E. Solver Details

The computational domain of the simulation extends from the anode through the channel and into the near-field plume region. A non-uniform orthogonal grid is used to span the computational domain with 101 grid points in the axial direction and 13 in the radial direction, as shown in Fig. 2.

The numerical model implements a fourth order Runge-Kutta scheme to solve the electron energy equation in order to update the electron temperature perpendicular to the magnetic field at each time step. The spatial derivatives are calculated using second-order central differencing. The boundary conditions used in this implementation are Dirichlet for the electric potential at both the anode and cathode. The temperature boundary conditions are Dirichlet at the cathode assuming constant electron energy injection, and Neumann at the anode assuming infinite diffusion.

A standard leap-frog technique is employed for the time advancement of heavy particles. For computational manageability, superparticles are used to represent large groups of neutrals and ions rather than individual particles. Since neutral and ion densities differ by orders of magnitude over the length of the domain, the size of the

superparticles vary with both space and species. The simulation is initialized with approximately 200,000 to 300,000 superparticles of each heavy particle species.

Due to the fast electron time scale relative to the ions and neutrals, the step size used for time advancement differs for each species. The ion and neutral time step is typically 25 ns, while the electron time step is on the order of 0.1 ns. Therefore, ions and neutrals are advanced in time after several electron iterations. On a 1.8 GHz Pentium 4 processor, the simulation completes 625 μs, or approximately five to ten "breathing mode" cycles, in two days.

III. Results and Discussion

The effect of cross-field mobility, discharge voltage, neutral wall scattering, background gas, and charge exchange collisions on the simulated results will be examined. The reference case will be taken as a 200 V simulation with an experimentally-based mobility, diffuse neutral wall interactions, and no background or collisions. In addition, a comparison will be made between the numerical results and experimental measurements in the Stanford Hall Thruster of neutral and ion axial velocity, plasma density, neutral density, potential, and electron temperature.

A. Cross-Field Mobility

Accurately representing electron diffusion in a numerical model is necessary in order to correctly describe the ionization and acceleration process. However, the experimentally observed axial electron current in a Hall thruster is greater than predicted by classical diffusion based on collisions with neutrals. Since a two dimensional model is unable to accurately predict the "anomalous" mobility caused by three-dimensional effects such as azimuthal fluctuations, implementation of an ad-hoc hall parameter is required.

Classically, cross-field electron mobility is given by:

$$\mu_{ez} = \left(\frac{1}{B_r}\right)\frac{1}{\omega_{ce}\tau} \qquad (6)$$

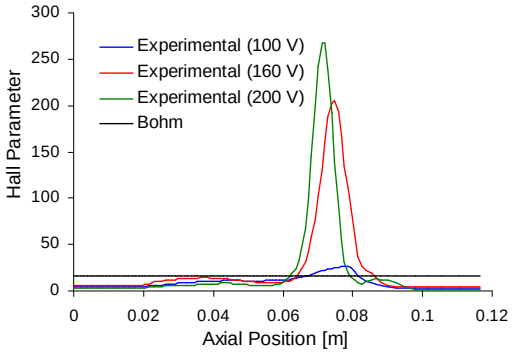

Figure 3. Bohm and experimentally measured Hall Parameter, $\omega\tau_{eff}$.

where B_r is the radial component of the magnetic field, ω_{ce} is the electron cyclotron frequency, and τ is the mean time between collisions. Therefore, electron mobility is inversely proportional to the Hall parameter, $\omega_{ce}\tau$.

According to the Bohm[6] model of electron diffusion, the effective Hall parameter is given by $\omega_{ce}\tau$ equals 16. A comparison of Bohm mobility with an axially-varying experimental Hall parameter measured by Meezan[7] is given in Fig. 3. As illustrated, the Bohm model fails to capture the significant reduction of cross-field mobility in the ionization region of the channel where the actual mobility is closer to the classical value.

As shown in Fig. 4, the experimental Hall parameter produces a steep potential drop near the exit plane of the thruster due to the decreased mobility. Using a constant Bohm Hall parameter produces a more gradual accelerating

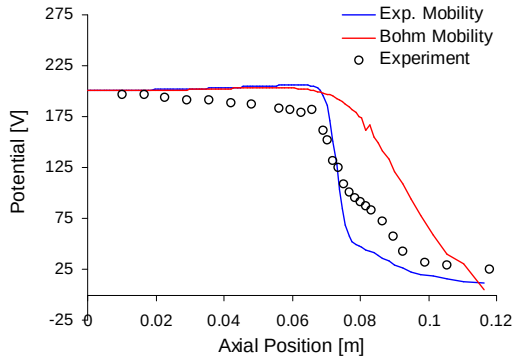

Figure 4. Comparison of experimental potential to simulated results using Bohm and experimental mobility.

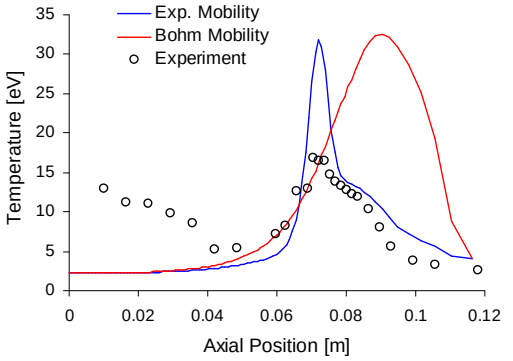

Figure 5. Comparison of experimental electron temperature to simulated results using Bohm and experimental mobility.

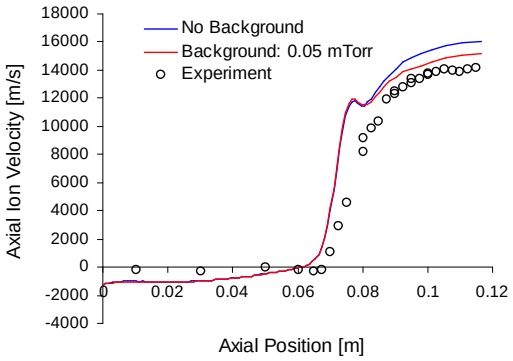

Figure 6. Comparison of experimental axial ion velocity to simulated results with and without background gas.

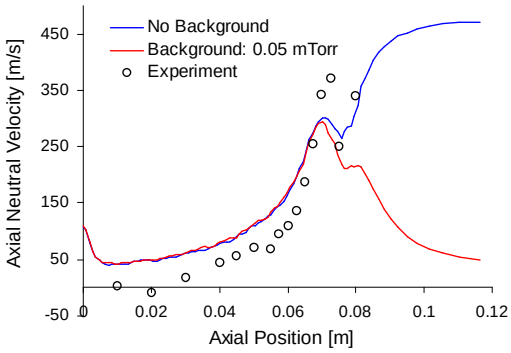

Figure 7. Comparison of experimental axial neutral velocity to simulated results with and without background gas.

potential which occurs almost entirely outside the channel, also shown in Fig. 4. Although both Bohm and experimental conductivity models fail to reproduce the measured potential, the experimental Hall parameter more accurately confines the acceleration zone resulting in improved simulated electron temperatures.

Bohm diffusion produces an electron temperature profile which peaks downstream of the experimentally observed location as shown in Fig. 5. However, implementation of an experimental mobility produces electron temperatures which peak at the expected location near the exit plane. The failure of the Bohm model is due in large part to the simulated electric field. For the experimental mobility case, the electric field is largest at the location of the maximum temperature as shown by the steep gradient of potential in Fig. 4. Since temperature is coupled to electric field through the joule heating source term in the energy equation, the location of the maximum electron temperature is correctly predicted for the case of experimental mobility. However, for the Bohm case, the electric field is less intense in the ionization zone and more intense in the near field than experimentally measured. As a result, the electron temperature is under predicted in the channel and over predicted in the plume. A primary factor contributing to the differing potential and temperature curves for the two conductivity models is the inclusion of the experimental mobility in the energy equation through thermal diffusivity in addition to the generalized Ohm's law.

An additional factor contributing to the shift in electron temperature is the increase in discharge current accompanying Bohm diffusion due to the lowered resistance. The enhanced current depletes the neutral population inside the channel through increased ionization resulting in less ionization-induced losses in the plume. Using both the Bohm and experimental Hall parameters, the peak electron temperature is nearly double the experimental maximum. Preliminary work suggests that improving the electron wall damping model is necessary to lower the simulated temperature to reasonable values.

B. Background Gas

In simulations of ground-based chamber tests, the inclusion of background gas is critical in order to accurately represent the neutral number density. The amount of neutral gas in the simulation is used to calculate the ionization rate, which is directly coupled to the plasma density and electric potential. In order to deduce the magnitude of background effects, background gas has been added to the reference case for comparison. Addition of background gas is accomplished by uniformly injecting neutral xenon particles into the simulation from the edges of the computational domain bordering the near-field region. A net one-way flux of $n\bar{c}/4$ is assumed with a half-Maxwellian velocity distribution normal to the injection surface.

The effect of background gas on axial ion velocity is shown in Fig. 6 with a total background pressure of 0.05 mTorr and a temperature of 300 K. Ingestion of neutral particles into the channel from the plume produces ions born at lower potentials than those created from neutrals injected from the anode. Therefore, the net effect of background gas is to lower the maximum axial ion velocity causing the simulated results to more closely match experimental measurements.

Despite the better agreement of axial ion velocity, addition of background gas currently has a negative effect on axial neutral velocity as shown in Fig. 7. Since the number density of the background gas is higher than that of neutral gas exiting the channel in vacuum, the flux of the two neutral populations approximately cancel despite the differing speeds. This cancellation causes the average neutral velocity to tend towards zero beyond the exit plane of the thruster. This dramatic decrease is not observed experimentally near the exit plane of the Stanford Hall thruster.

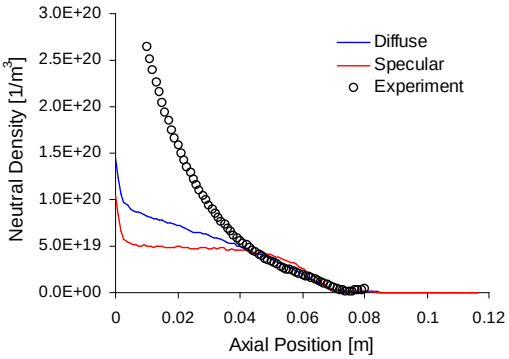

Figure 8. Comparison of experimental neutral number density to simulated results using diffuse and specular neutral wall interactions.

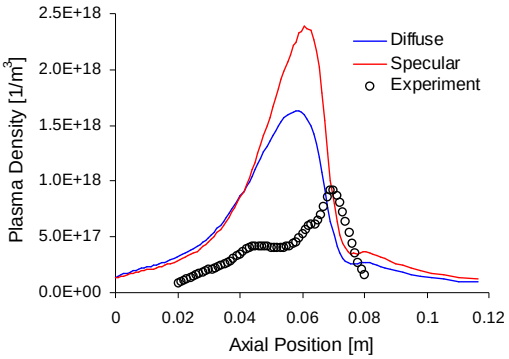

Figure 9. Comparison of experimental ion number density to simulated results using diffuse and specular neutral wall interactions.

It is expected that lowering the overestimated plasma density through improved wall physics will increase the neutral density exiting the channel, causing the effect of background gas to be less significant.

C. Neutral Wall Interactions

The way in which neutral particles reflect off the channel walls directly affects the neutral velocity profile and the neutral number density in the entire computational domain. Since neutral density is coupled to plasma density through ionization, neutral wall interactions are relevant to the overall accuracy of the simulation. The two primary models for neutral wall interactions are specular and diffuse scattering. Each method is implemented separately in the simulation and the results are compared with experimental measurements to determine which model better reflects reality. Specular scattering is accomplished by reversing the radial component of velocity when a particle reaches the channel boundaries. In diffuse scattering, the particle thermalizes at the wall temperature and is reemitted with a random angle and speed chosen using a Maxwellian one-way velocity distribution function.

As shown in Fig. 8, specular scattering produces a neutral number density that is far more uniform inside the channel than diffuse scattering. This uniformity in number density results in a more constant neutral velocity. As illustrated by Fig. 7, experimentally the neutral velocity is observed to accelerate from zero near the anode to approximately 300 m/s near the exit, which is in better agreement with the diffuse scattering model. Although both diffuse and specular scattering fail to reproduce the measured number density near the anode, the experimental uncertainty in this region is large. For the outer half of the channel, the diffuse scattering simulation matches experimental observations well, whereas the specular scattering overestimates the neutral number density. As a result of the increased neutral density in the ionization zone (Fig. 8), specular scattering produces a larger plasma density as shown in Fig. 9. The overestimation of plasma density relative to experiment using both diffuse and specular models is likely due to the over predicted electron temperature (Fig. 5).

D. Charge Exchange Collisions

In the reference case simulation, all collisions between heavy particles are ignored. While this approach may be approximately valid for elastic collisions in which the velocity distribution is not significantly altered by particle interactions, the same assumption does not hold for charge exchange collisions. Since the velocity distribution of neutrals and ions differ greatly, charge exchange scattering events result in new populations of each species. In the plume of a Hall thruster, charge exchange collisions between fast ions and slow neutrals typically produce slow ions and fast neutrals. The slow ions may be influenced by the potential fields surrounding the Hall thruster and accelerate back toward the spacecraft leading to sputtering and deposition. Therefore, in an attempt to improve the accuracy of the simulation, charge exchange collisions have been added over the entire computational domain.

Experimental measurements by Pullins[8], et al. are used to determine the total cross section as a function of energy:

$$\sigma_{Xe-Xe^+} = \left(-23.3\log_{10}(g) + 188.81\right) \times 1.1872 \ \text{Å}^2 \tag{7}$$

where $\sigma_{Xe\text{-}Xe+}$ is the total charge exchange cross section and g is the relative velocity.

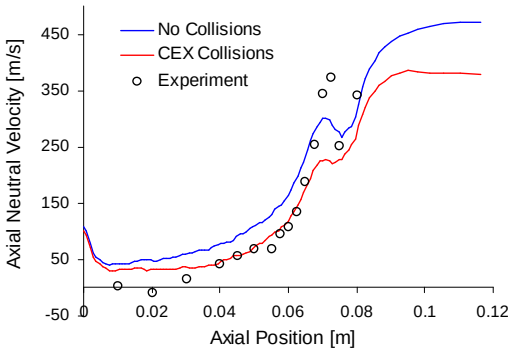

Figure 10. Comparison of experimental axial neutral velocity to simulated results with and without charge exchange collisions.

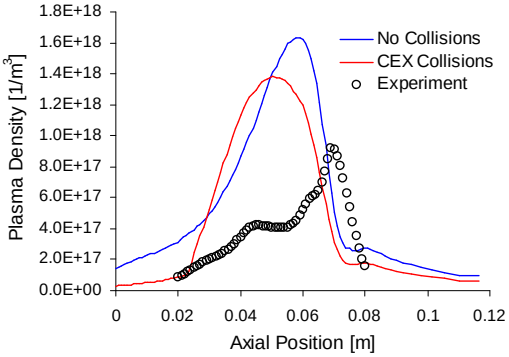

Figure 11. Comparison of experimental plasma density to simulated results with and without charge exchange collisions.

Only neutrals and ions in the same computational cell are eligible to collide. Collision partners from within a cell are chosen using the pair selection scheme described by Bird.[9] First X ion-neutral pairs are chosen from within a cell.

$$X = n_i n_n (\sigma g)_{\max} V \Delta t \tag{8}$$

where n_i is the ion density, n_n is the neutral density, $(\sigma g)_{\max}$ is the maximum value of the total cross section multiplied by the relative velocity for all possible pairs, V is the volume of the cell, and Δt is the time step. Once X partners are chosen, they are collided with probability, P.

$$P = \frac{\sigma g}{(\sigma g)_{\max}} \tag{9}$$

Differing superparticle weights are accounted for in choosing collision pairs.

On average, a neutral superparticle is two orders of magnitude larger than an ion superparticle. Therefore, if a charge exchange collision is determined to take place, the larger particle (typically the neutral) is divided into a small particle the size of the collision partner and a large particle equal to the remainder. Since the most probable scattering event involves very little momentum transfer, the pre-collision velocities of the ion and neutral are exchanged. After the collision takes place, the small and large neutral particles are recombined to prevent an excessive number of particles from forming within the computational domain. While momentum is conserved at each time step using this method, approximately 3.5% of the pre-collision energy is lost per collision in recombining the particles. In future simulations, attempts will be made to resolve this inconsistency.

A comparison of axial neutral velocity with and without charge exchange collisions is shown in Fig. 10. As shown, the addition of charge exchange collisions produces better agreement with experiment inside the channel, and worse agreement near the exit. Without the inclusion of background gas, few collisions occur in the plume since the relative velocity between the species is high and the densities are low. Therefore, most of the charge exchange collisions take place in the middle of the channel where the plasma density and total cross section are at a maximum. As shown in Fig. 6, in this region the simulated ions are traveling back toward the anode. Therefore, charge exchange collisions in this region result in ions traveling at the thermal wall velocity and neutrals traveling toward the anode. As a result, charge exchange collisions have the effect of lowering the axial neutral velocity in the channel.

In addition to affecting neutral velocity, charge exchange collisions also alter the plasma density. Despite the lower average neutral velocity in the channel (Fig. 10), charge exchange collisions in fact decrease the neutral density in this region by creating a new population of neutral particles with increased axial velocity in the reverse direction. By lowering the neutral number density in the ionization region, charge exchange collisions decrease the peak plasma density as shown in Fig. 11. Since these collisions typically decrease the axial component of ion velocity inside the channel, they also impede the backflow of ions resulting in a significant reduction of plasma density near the anode and a shift of the peak location.

E. Discharge Voltage

The robustness of the numerical model has been tested through variation of the applied discharge voltage. The simulation was run at 100 V, 160 V, and 200 V corresponding to discharge voltages at which electron mobilities have been experimentally determined. A comparison of simulated versus experimentally measured discharge current at the three voltages is shown in Fig. 12.

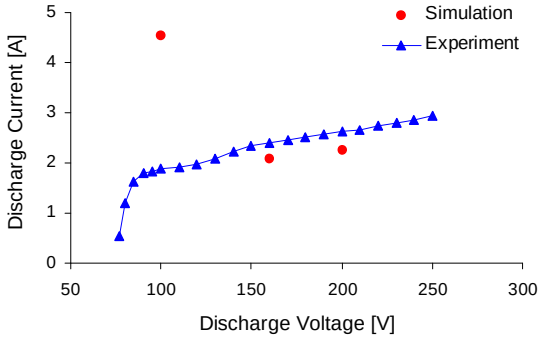

Figure 12. Simulated and experimentally measured I-V curves.

While the simulation is reasonably adept at predicting results at 160 V and 200 V, the differences between experiment and simulation grow at lower voltages suggesting that new physics needs to be added for these conditions. Another possible cause of the anomalous point at 100 V is error in the experimental mobility. The experimentally determined hall parameter is given by the following expression assuming negligible electron pressure effects:

$$\omega\tau_{eff} = \frac{J_{e\theta}}{J_{ez}} = \left(en_e \frac{B_r}{E_z}\right) \Big/ \left(\frac{I_a}{A} - en_e u\right) \tag{10}$$

where $J_{e\theta}$ is the current density in the azimuthal direction, J_{ez} is the current density in the axial direction, and A is the cross sectional area of the channel. Although axial ion velocity, u_i, discharge current, I_a, and radial magnetic field, B_r are known with reasonable experimental certainty, the possibility for error is much greater in plasma density, n_e, and axial electric field, E_z. If cross-field mobility is recalculated at 100 V by doubling the experimental plasma density, the discharge current decreases to approximately 2.5 Amps and the plasma properties are in better agreement with experiment, confirming the simulation sensitivity to effective hall parameter.

F. Particular Features

As shown by the axial ion velocity in Fig. 6, in addition to reproducing the overall acceleration process with reasonable accuracy, the simulation also captures subtle physical phenomena observed experimentally. The simulation predicts a backward acceleration of ions toward the anode upstream of the ionization zone. This characteristic of the ion velocity has been experimentally observed in a number of Hall thrusters including the Stanford Hall thruster. At 200 V, the reference case simulation produces average velocities on the order of 1000 m/s in the reverse direction near the anode. Experimentally, a net backflow is observed at the same operating conditions, however the magnitude of the reverse flow is a factor of five lower than predicted by the simulation.

Also in Fig. 6, the simulation predicts a dip in the ion velocity near the exit plane. While this dip is not apparent at 200 V, a slight decrease in the acceleration is observed near the same location. As reported by Hargus[10], a more noticeable kink is apparent in the axial ion velocity of the Stanford Hall thruster at higher operating voltages. The feature is likely a results of the decreased accelerating potential in this region (Fig. 4) being unable to overcome the axial velocity losses due to wall interactions and ionization. A consequence of the sudden decrease in ion velocity is a slight increase in the simulated plasma density at the same location as shown in Fig. 9.

Another experimentally observed phenomena which the simulation is able to reproduce is a decrease near the exit plane of the axial neutral velocity, as shown in Fig. 13. The shape of the axial velocity curve is influenced by the ionization rate, which selectively removes slow neutrals from the distribution, and diffuse wall interactions, which impede the neutral flow. After the accelerating ionization influence drops off as shown in Fig. 13, the wall interactions cause the neutral velocity to fall. Near the exit plane the average velocity increases once again due to a lack of particle flux in the opposing direction.

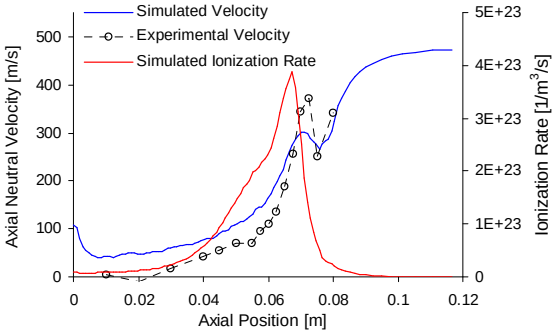

Figure 13. Simulated ionization rate and neutral velocity for the reference case vs. experimental neutral velocity.

IV. Conclusion

It has been shown that an experimentally measured Hall parameter is an effective way of describing the anomalous nature of electron cross-field mobility in a Hall thruster. The experimental mobility, which captures the classical behavior near the ionization zone, produces better simulated values of plasma properties than the constant Bohm model. Although the simulated electron temperature and plasma densities are higher than experimentally observed, it is believed that implementation of a more accurate wall damping model including current saturation effects as described by Barral[11] will bring the simulated values closer to experiment. Preliminary work at increasing the damping has shown this to be the case, however further work is required to improve simulation stability.

This work has also shown that diffuse neutral wall interactions produce better neutral density and velocity profiles than specular scattering. Whereas specular reflection results in a more uniform neutral density and velocity inside the channel, diffuse scattering predicts the experimentally observed phenomena of steadily decreasing number density and increasing velocity. Inclusion of charge exchange collisions also brings the simulated results closer to experiment by lowering the total plasma density and further decreasing the velocity of neutral particles near the anode. Simulation of background gas has the positive effect of lowering the final axial ion velocity. However, at present, the background effect is over predicted in neutral velocity due to the large simulated electron temperature.

One of the key successes of this numerical model is the ability to reproduce subtle experimentally observed features. Although the phenomena are exaggerated in the simulation, the model predicts a backflow of ions near the anode and a kink in axial ion velocity near the exit plane. In addition, the simulation accurately reproduces the exact location of an experimentally measured dip in axial neutral velocity caused by the counteracting influences of ionization and diffuse wall scattering.

Acknowledgments

This research was supported by the Air Force Office of Scientific Research. Stipend support for M. Allis was provided through a fellowship from the National Science Foundation. N. Gascon was partially supported by a fellowship from the European Space Agency. E. Fernandez acknowledges the Center for Turbulent Research for supporting this work and K. Mahesh for valuable assistance is the early stages of code development.

References

[1]Fernandez, E., Cappelli, M. A., Mahesh, K., "2D Simulations of Hall Thrusters," *CTR Annual Research Briefs*, 1998, pp. 81.

[2]Fife, J. M., "Two-Dimensional Hybrid Particle-in-Cell Modeling of Hall Thrusters," S.M. Thesis, Aeronautics and Astronautics Dept., Massachusetts Institute of Technology, Cambridge, MA, 1995.

[3]Fife, J. M., "Nonlinear Hybrid-PIC Modeling and Electrostatic Probe Survey of Hall Thrusters," Ph.D. Dissertation, Aeronautics and Astronautics Dept., Massachusetts Institute of Technology, Cambridge, MA, 1998.

[4]Birdsall, C. K, and Langdon, A. B., *Plasma Physics via Computer Simulation*, IOP Publishing Ltd., Briston, England, 1991, Chap. 16.

[5]Dugan, J. V. and Sovie, R. J., "Volume Ion Production Costs in Tenuous Plasmas: A General Atom Theory and Detailed Results for Helium, Argon and Cesium," NASA TN D-4150.

[6]Bohm, D, Burhop, E.H.S. Massey, H.S.W, "The Use of Probes for Plasma Exploration in Strong Magnetic Fields", in "The Characteristics of Electrical Discharges in Magnetic Fields," Guthrie A., Wakerling R.K., ed., McGraw-Hill, 1949, pp. 13-76.

[7]Meezan, N. B., Hargus, W. A., and Cappelli, M. A., "Anomalous Electron Mobility in a Coaxial Hall Plasma Discharge," *Physical Review E*, Vol. 63, 026420, 2001.

[8]Pullins, S., Chiu, Y., Levandier, D. and Dressler, R., "Ion Dynamics in Hall Effect and Ion Thrusters: Xe^+ + Xe Symmetric Charge Transfer," *AIAA Paper* 00-0603, Jan. 2000.

[9]Bird, G. A., *Molecular Gas Dynamics and Direct Simulation of Gas Flows*, Oxford University Press, Oxford, 1994, Chap. 11.

[10]Hargus, W. A., "Investigation of the Plasma Acceleration Mechanism within a Coaxial Hall Thruster," Ph.D. Dissertation, Mechanical Engineering Dept., Stanford University, Stanford, CA, 2001.

[11]Barral, S., Makowski, K., Peradzynski, Z., Gascon, N., Dudeck, M., "Wall Material Effects in Stationary Plasma Thrusters II: Near-Wall and Inner-Wall Conductivity," *Physics of Plasmas*, Vol. 10, No. 10, Oct. 2003, pp. 4137.